Received: 10 January 2024 | Revised: 6 February 2024 | Accepted: 7 February 2024

DOI: 10.1111/jmi.13279

Journal of Microscopy RMS

THEMED ISSUE ARTICLE

Investigations on lightweight concrete by in situ compression tests using high-resolution computed tomography (μ-CT)

Cristin Umbach | **Bernhard Middendorf**

Department of Structural Materials and Construction Chemistry, University of Kassel, Kassel, Germany

Correspondence
Cristin Umbach, Department of Structural Materials and Construction Chemistry, University of Kassel, Mönchebergstr. 7, 34125 Kassel, Germany.
Email: c.umbach@uni-kassel.de

Abstract

The fracture behaviour of concrete is studied in various micro- and macro-damage models. This is important for estimating serviceability and stability of concrete structures. However, a detailed understanding of the material behaviour under load is often not available. In order to better interpret the fracture behaviour and pattern, images of lightweight concrete were taken using a high-resolution computed tomography (μ-CT) scanner. The samples were loaded between the taken images and the load was kept constant during the measurement. This study describes the method used and how the data set was analysed to investigate displacements and cracks. It has been shown that displacements and damage to the concrete structure can be detected prior to failure, allowing conclusions to be drawn about the structural behaviour. In principle, the μ-CT measurement can be used to examine different kinds of concrete as well as other systems with inorganic binders and to compare the fracture behaviour of different systems.

KEYWORDS

crack development, high-resolution computed tomography, in situ compression test, lightweight concrete, porosity

1 | INTRODUCTION

The compressive strength of concretes is one of the basic characteristics used to classify concretes into performance classes. Known behaviour is expected in both the stress–strain relationship and the fracture pattern. If the concrete meets these properties, it can be used according to the applicable standards. For newly developed special concretes, this known behaviour does not always apply. It is therefore important to learn more about the fracture behaviour of concrete. High-resolution computed tomography (μ-CT) is one way to look at internal structures in detail. It uses differences in density to identify individual components and make the microstructure visible.

In recent years, a number of micro-scale damage models have been developed[1–3] A correlation between work and stiffness (Young's modulus) as well as crack volume has been discovered. These data can be used to predict damage.[4] Almost all of the results were obtained using ex-situ loading, where the elastic part of the deformation has to be reduced again in order to measure the samples, for example, using computed tomography (CT). In particular,

the relationship between crack area and work is consistent with the theory of linear-elastic fracture mechanics (LEFM) described in Bažant et al.[5] For the plastic deformations that can be observed in concretes, this approach is only partially applicable, since a brittle failure mode is assumed.

A μ-CT scan before or after failure is not sufficient to reveal interactions or changes in the microstructure. Therefore, an in situ set-up was chosen in this work. This can be used to observe displacements and cracks before the maximum load is reached, thus characterising the material behaviour under load. The load is held constant during a scan and then applied again after it. Finally, the 3D images can be analysed under different loads to gain an improved understanding of the material.

2 | HIGH-RESOLUTION COMPUTED TOMOGRAPHY

Computed tomography can be used to show density differences in a 3D image. The basic function of computed tomography is the reconstruction of an object from its projections. The object is radiated with X-rays at different angles and the projections are recorded on a detector.

In the following, the measurement method of high-resolution computed tomography (μ-CT) is described in detail. This method is defined by a resolution in the one- to two-digit μm range. The used device is a Xradia 520 Versa (Zeiss Microscopy, Oberkochen, Germany) and has a spatial resolution of 0.7–50 μm. To visualise cracks in material samples in three dimensions, high resolutions in the range of a few micrometers are required. The resolution is influenced by several factors of the physical principle. Therefore, the measurement principle will be discussed in more detail in the following part. The procedure for the in situ tests is thereafter explained.

2.1 | Measuring principle

The measuring principle of computed tomography is based on the radiation of objects with X-rays from different angles and the subsequent reconstruction of the projections into a three-dimensional data set. Thereby, computed tomography detects density differences within the object.

Computed tomography is described in detail.[6] In the following, the topics of filtering, detector, geometric magnification, resolution, reconstruction and artefacts are explained briefly. These factors affect measurement quality, resolution and recording time. In order to observe and evaluate cracks and displacements in concrete, the measurement quality and resolution must be chosen in such a way that this form of evaluation is possible. Furthermore, the measurement time must be as short as possible to minimise retarded ductile and creep deformations during the scan. In the ideal state, these deformations should be significantly smaller than the resolution, so that the reconstruction of the images works correctly.

2.1.1 | Filter

In radiographic transmission, the attenuation of X-rays depends on the wavelength. In general, low-energy X-rays, that is, radiation with a longer wavelength, are attenuated more when passing through matter. As a result, the radiation spectrum is shifted to higher energies after attenuation. This is called beam hardening. Beam hardening produces artefacts in the reconstructed data sets because the reconstruction algorithms assume monochromatic radiation. To minimise this effect, the X-rays are filtered. For this purpose, aluminium or copper filters are mounted on the source side. The filters pre-harden the radiation; that is, they reduce the number of X-ray quanta and increase the average radiation energy.

Choosing the appropriate acceleration voltage and filter is important to obtaining a high-quality image. This will determine how much background noise will be in the image. If there is a lot of background noise, it may be difficult or even impossible to evaluate the images. Therefore, in some cases, test exposures with different parameters are necessary to find the appropriate quality level.

2.1.2 | Detector with coupled optics

X-ray detectors convert the remaining radiation into a measurable signal. Detectors in computed tomography measure the spatial intensity distribution and radiation power. The radiation power reaching the detector must exceed a threshold to ensure sufficient image quality and resolution. The Xradia 520 Versa has four scintillation detectors with linked optics (0.4×, 4×, 20×, 40×). Scintillation detectors have two coupled components: a scintillator medium and a photon detector in the form of a CCD detector. In the scintillator medium, short wavelength X-rays are converted to long wavelength radiation (light). This light passes through lenses with different magnifications and is recorded in a charge-coupled device (CCD) with a pixel field of 2048 × 2048.

2.1.3 | Geometric magnification

Due to the variability of the positioning of the source and detector in relation to the object and the cone beam, the geometric magnification can also be used for computed

tomography imaging via the beam set.

$$\text{geometric magnification} = \frac{\text{SOD} + \text{ODD}}{\text{SOD}}$$

SOD: Source-Object-Distance; ODD: Object-Detector-Distance.

The total magnification is the result of the multiplication of the geometric magnification and the optical magnification.

2.1.4 | Resolution and image size

The image size of the field of view (FOV) is limited by the pixel field at the detector and the resolution x. The FOV can be a maximum of 2048 times the resolution. This means that for a constant resolution of 1 μm, the FOV has a size of 2048 mm. The FOV can be further reduced by grouping pixels (binning) on the detector. One solution to increase the measurement range is stitching. Stitching is the process of adding two or more images together. For this method, the two images taken with the same measurement parameters must have an overlapping area, and the same grey values must be used to calculate the same intensities during reconstruction.

2.1.5 | Reconstruction

Reconstruction of X-ray images taken at different angles is an automated process. Several parameters are determined and applied to the image. The two important values are centre shift and minimum and maximum grey values. The latter results in the values for black (0) and white (65535). The filtered back-projection algorithm is used for reconstruction of the recorded projections.

2.1.6 | Image quality

Due to the many interactions and data transfers, μ-CT images can quickly lead to image quality problems if data is lost due to transfer processes or unintentional downscaling. If these factors are excluded, the image quality can be influenced by the measurement settings. The following information refers to the Xradia 520 Versa.

The sample size should be as close as possible to the desired FOV. It may be necessary to prepare partial samples for this purpose.

An appropriate acceleration voltage and exposure time must be selected for the X-rays. For high-quality μ-CT images, more than 5000 signals (counts) should be counted on the detector in each area. In addition, the transmission through the sample should be between 20% and 35% and a filter suitable for the radiation should be used for pre-hardening.

For a usable μ-CT image, an angular range of at least 180° should be covered. However, to minimise artefacts and improve image quality, 360° is preferable. The number of exposures is also important for image quality. For sufficiently high image quality, 1601 exposures are recommended. If this is not sufficient for the desired display quality, the number of images can be increased. The odd number of images is necessary so that the angle 0°/360° (image 1/image 1601) and the angle 180° (image 801) are exactly opposite to each other and should therefore result in the same projection. This means that two images are always exactly opposite each other when measuring 360°.

2.1.7 | Used parameters

The focus of this study was to examine concrete samples with porous lightweight aggregates under different load levels in 3D images. This required images of high quality and resolution for reproducible evaluation. The selection of the appropriate settings for source, detector and sample position was essential for this.

On the other hand, the measurement time had to be as short as possible in order to minimise deformation processes under stable load. This was achieved by reducing the acquisition angle to 180°, the number of images to 801 and the pixel grouping to binning 2.

A list of the selected settings, taking into account the additional edge parameters provided by the in situ load frame, is summarised in Table 1.

2.2 | In situ measuring element

Using the in situ method, the concrete samples are loaded progressively between measurements, allowing crack growth within the sample to become visible. The advantages of in situ loading are

- measurement without intermediate unloading
- the same area is always measured
- crack growth can be observed between measurements

Figure 1 shows the Microtest CT5000RT load frame (Deben UK Ltd., Woolpit, United Kingdom) placed in μ-CT. The sample position and load are also shown schematically.

TABLE 1 Used settings for image acquisition.

Parameter		Setting
Source	Voltage	140 kV
	Power	10 Watt
	Position	–100 mm
	Filter	HE 1 (copper)
	Exposure time	10 s
	Angel of radiation cone	1.45°
Detector	Type	Objective 4× + CCD
	Position	35 mm
	Binning	2
Sample	Position x	0 μm
	Position y	13,000 μm
	Position z	0 μm
Acquisition	Field of view (FOV)	5120 μm
	Resolution	5 μm
	Acquisition angle	180°
	Number of projections	801
	Type of reference	Single image
Reconstruction	Type of reconstruction	Filtered back-projection

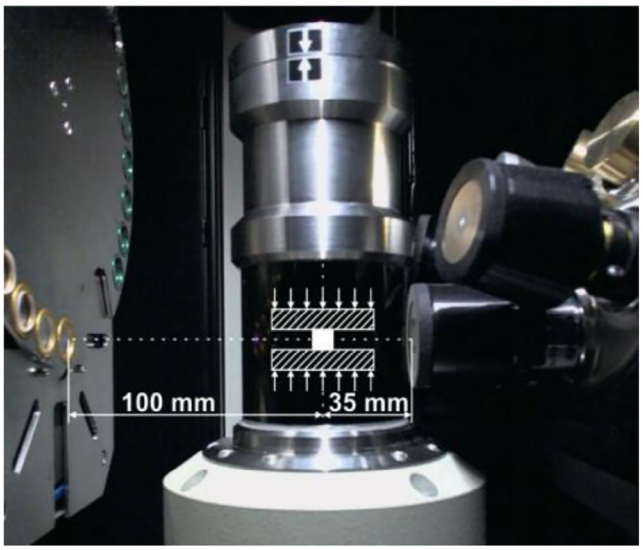

FIGURE 1 Positioning of the μ-CT-scanner with Microtest CT5000RT load frame.

2.2.1 | Measuring times

The measurement times (Figure 2) are selected according to different defined stress conditions. The first measurement (1) is performed in the unloaded condition. This measurement serves as a reference for the evaluation of the 3D data.

The second measurement (2) takes place in the linear-elastic range at 30% of the maximum stress σ. In this scan,

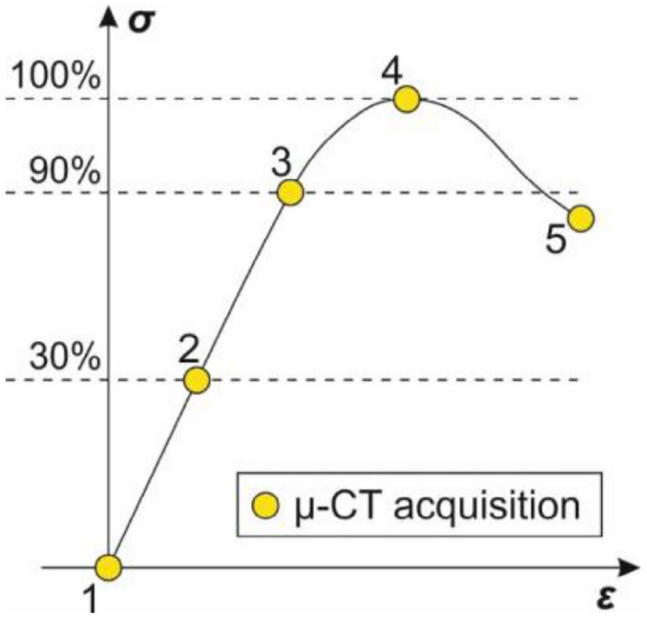

FIGURE 2 Measuring points for the μ-CT acquisition.

the load is kept constant for the first time over the measurement time. This can result in delayed elastic or delayed plastic deformations. Therefore, all scans should be performed as quickly as possible. The slope of the load curve in the σ-ε diagram can be used to determine the Young's modulus of the undamaged material.

The third measurement (3) is taken at 90% of the maximum stress, that is, at the end of stable crack growth. The first cracks and damage in the lightweight aggregate should be visible here. The Young's moduli can also be compared.

The fourth measurement (4) is taken at maximum stress. As this is in the unstable crack growth region, it is not always possible to record this measurement, as some of the samples failed during the measurement period. In this case, the sample was completely destroyed as the load frame was designed to hold the load. As the load that could be applied decreased, the distance between the load plates was reduced (to regain the desired force again) to a minimum of 5 mm.

The 5th measurement (5) records the final state of the sample. The load is stopped during this measurement. To maintain the elastic deformation, the load plates must not be opened.

2.2.2 | Influences of the method on sample size and resolution

The Microtest CT5000RT load frame from Deben was used for loading (Figure 1). This is compatible with the software

of the used μ-CT and allows tensile and compression tests with a maximum load of 5000 N to be performed. A sample chamber with a diameter of 42 mm is available for compression tests. The height at which the samples can be loaded is between 5 and 15 mm. By limiting the sample space and assuming that the concrete samples achieve a strength of 70–100 MPa, the maximum area that can be loaded can be calculated as follows:

$$\sigma = \frac{F}{A} \rightarrow A = \frac{F}{\sigma} = \frac{5000\ \text{N}}{100\ \text{MPa}} = 50\ \text{mm}$$

This gives the following maximum dimensions for the cube and cylinder geometries:

$$\text{Cube:} \quad A = a^2 \rightarrow a = \sqrt{A} = \sqrt{50\ \text{mm}^2} = 7.07\ \text{mm},$$

$$\text{Cylinder: } A = \pi \times r^2 \rightarrow r = \sqrt{\frac{A}{\pi}} = \sqrt{\frac{50\ \text{mm}^2}{\pi}}$$
$$= 3.99\ \text{mm} \rightarrow \infty = 7.98\ \text{mm}.$$

To visualise cracks in the structure, the resolution should be no greater than 5 μm. The grains, which can be as small as 0.1 mm, should be displayed with as many voxels (three-dimensional pixels) as possible to ensure differentiation between air voids and expanded glass. This allows the following FOVs to be set for different pixel groupings:

$$\text{Binning 1:} \quad 5\ \mu\text{m} \times 2048\ \text{Pixel} = 10,248\ \mu\text{m} = 10.2\ \text{mm}$$

$$\text{Binning 2:} \quad 5\ \mu\text{m} \times 1024\ \text{Pixel} = 5120\ \mu\text{m} = 5.1\ \text{mm}$$

$$\text{Binning 4:} \quad 5\ \mu\text{m} \times 512\ \text{Pixel} = 2560\ \mu\text{m} = 2.6\ \text{mm}$$

To achieve the desired resolution, the lens and the position of the X-ray source and detector must be determined. The detector and X-ray source can be moved up to 35 mm from the sample. The 4× objective is used to achieve the desired resolution of 5 μm. Pixel grouping (binning 2) is used to reduce the exposure time (= measurement time). This results in an image size of 5120 μm × 5120 μm. With these parameters, a geometric magnification of 1.35 is required. The geometric magnification is calculated using the equation presented in Section 2.1.3. This results in the positions of the detector and the X-ray source:

Source-Object-Distance: 100 mm
Object-Detector-Distance: 35 mm

2.2.3 | Influences of sample size on strength

Typically, the scaling effect leads to higher strengths with smaller geometry.[5,7,8] However, in the scaling effect studies, the sample size is reduced to a minimum of 25 mm. Smaller samples are not considered. It is only assumed that the strength continues to increase or remains the same.

For very small samples, the increased surface area to volume ratio (specific surface area) must also be considered. The moulded surfaces have a different composition than the material inside the sample. In lightweight concrete, the cement paste layer on the outside has a higher strength than the lightweight aggregate. This holds the concrete together and increases its strength (Figure 3). In normal strength concrete, the wall effect reduces the strength.[8] Due to the larger specific surface area, this effect is increased in small samples. In order not to influence the failure mode of the sample due to the wall effect, the samples for the μ-CT tests were taken as drill cores from larger samples. This meant that all individual samples were taken from one sample.

Based on the requirements determined above, 8 mm diameter/high drill core was selected as the sample geometry. The sample was measured slightly off-centre to show the crack development at the edge and in the centre (Figure 4).

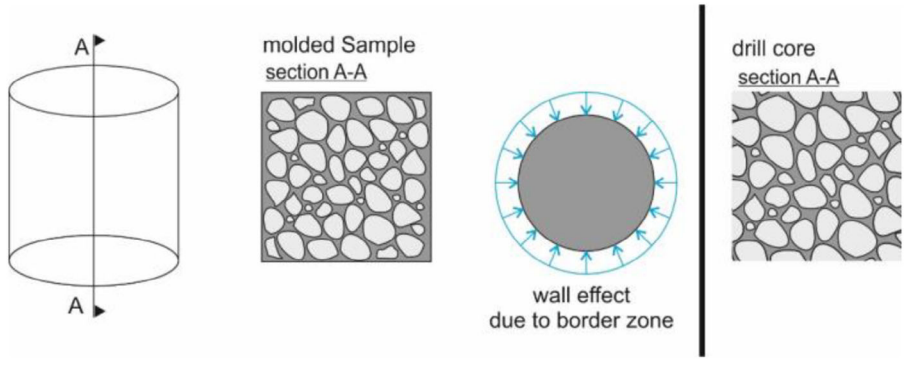

FIGURE 3 Border zone for moulded samples and drill cores.

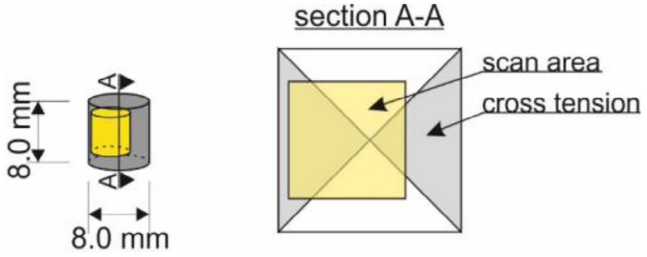

FIGURE 4 Sample positioning in the μ-CT scanner for acquisition.

TABLE 2 Composition of measured ultrahigh-performance lightweight concrete.

Raw material	Unit	UHPLC
Cement Holcim Sulfo 5R	kg/m^3	771.90
Silica fume Sika Sillicoll P uncompacted	kg/m^3	163.65
Superplasticizer Sika ViscoCrete 2810	% bwoc[a]	3.9
Hydrophobing agent Sika Control AE-10	% bwoc[a]	2.0
Quartz flour Quarzwerke Millisil W12	kg/m^3	199.00
Quartz sand Quarzwerke G32	kg/m^3	627.76
expanded glass Poraver 0.1–0.3 mm	kg/m^3	29.43
expanded glass Poraver 0.25–0.5 mm	kg/m^3	67.61
Parameters of mix design		
Water/binder ratio	kg/kg	0.21
Dry bulk density	kg/m^3	1.90

[a]By weight of cement.

2.2.4 | Concrete and sample preparation

The concrete used for the investigations is an ultrahigh-performance lightweight concrete (UHPLC), which is described and characterised in detail in Umbach et al.[9] In addition, Table 2 shows the composition with density class D2.0, which is presented in the results.

All produced samples were demoulded after 24 h and stored at 20°C and 65% RH until testing. The samples for the μ-CT tests were drilled from cubes of 15 cm edge length after 1-week storage using a core drilling machine (Figure 5). The cores were 8 mm in diameter and approximately 20–50 mm in length. Seven days later, samples of 8 mm in length were cut from these cores using a precision cutter (Buehler; IsoMet Low Speed). An earlier processing time was not possible because the cores would have damaged. After sawing, the samples were dried for 24 h at 40°C and stored for one day at 20°C and 65% relative humidity. This was to ensure that the bulk density of the concrete could be determined during subsequent measurement and weighing. Since the samples had a height difference of about 0.1 mm due to inaccuracies during drilling and sawing, they were aligned with a mixture of Portland cement (Holcim Sulfo 5R (CEM I 52.5 R-SR3)), alumina cement (Imerys Aluminates; Ciment Fondu), and quartz powder (Quarzwerke; W3). The use of alumina cement results in a setting time of approximately 4 h and a rapid strength development of > 50 N/mm^2 after 24 h and > 50 N/mm^2 after 48 h (determined on prisms according to DIN EN 196-1[10]). In combination with Portland cement, the setting time is reduced to 10–30 min. The quartz powder was used instead of a fine grained aggregate. This allows testing within the next few days. The thinnest possible layer of cement paste with a water/cement ratio of 0.46 was applied to both sides of the samples for adjustment. This resulted in a total height of approximately 8.1 mm. To prevent the thin levelling layer from peeling, a 24-h waiting period was applied before the load was removed from the samples. This allowed five samples to be levelled in one day. After 25 days, 5 samples were tested in the load frame with a displacement controlled test (0.1 mm/min) to determine the stress–stain curve and define the load levels.

3 | ANALYSIS METHODS

The 3D data sets were analysed using the Avizo 9.5 (Thermo Fischer Scientific Inc.) program. This program provides many methods for analysing 3D data. The general procedure for analysis is as follows:

- Define the region of interest (ROI)
- Filtering
- Segmentation
- Mathematical analysis of segmented objects
- Evaluation.

Defining a region of interest (ROI) can be useful when a specific area of the measurement is of interest. To do this, the data set is trimmed so that, for example, rectangular areas can be cut out of the cylindrical data set. Care must be taken not to 'cut up' any voxels. This means to always cut at the boundary from voxel to voxel, otherwise some analysis methods cannot be performed. In any case, the boundary areas of the measurement should be removed, as there are many artefacts. In this work, the data sets were also trimmed at the edges for analysis to avoid the influence of artefacts.

3.1 | Non-Local-Means Filter

Filtering data sets is used to highlight or emphasise certain features of the structures. This is done by transforming the image and extracting the desired information or improving the appearance of the data. For example, filters can be used to reduce noise or increase contrast.[11]

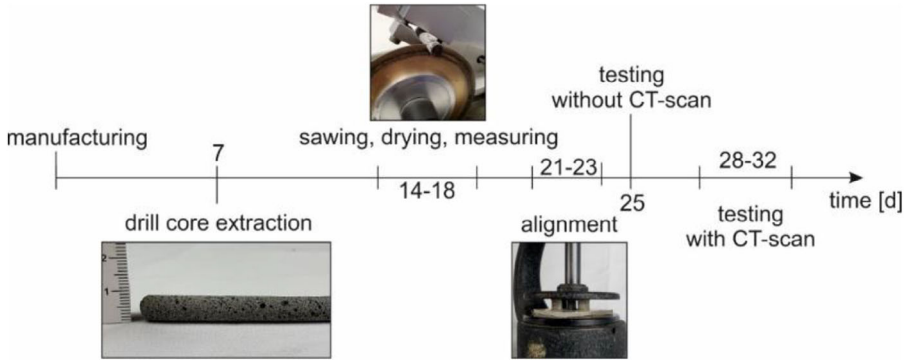

FIGURE 5 Sample preparation from manufacturing to testing.

Mathematically, a filter is an operator Φ that plots an input function *f* to an output function *g*. Filters are divided into two categories, linear and nonlinear. The nonlinear filters are described by more complex algorithms that do not belong to a specific theoretical group. Therefore, a separate definition must be given for each type of nonlinear filter.

The Non-Local Mean Filter is one of the nonlinear filter types. Unlike the usual algorithms that take the average of a group of pixels, this filter compares all pixels to the currently viewed pixel. This means that an average value of all pixels is calculated, weighted according to the similarity of the pixel to the target pixel.[12] Since this procedure is very complex and therefore time-consuming, this filter is used in a limited form in most programs.

Figure 6 shows a sectional view of a data set. The corresponding histograms are shown next to the sectional images. Before filtering, the image is noisy and the histogram is broad and not differentiated. After filtering with the NLM filter, the noise is minimised, but the edges and contrast are preserved, as can be seen in the histogram. After filtering, two clear peaks can be seen, which in this case can be used to separate and evaluate matrix and air voids.

3.2 | Otsu theresholding

Segmenting the data set is the most important step in preparing for analysis. It divides the dataset into non-overlapping regions. Segmentation is the most error-prone step, because setting a threshold affects whether a pixel/voxel belongs to one region or another. Therefore, in addition to manual methods, there are also automated methods. Basically, there are three different methods for segmenting data: thresholding, contour following, and region growing. An automated thresholding method, Otsu Thresholding, was chosen for this study.

All thresholding methods work by specifying a threshold value *k*. The threshold value is used to transform the greyscale image *f*(*x*,*y*) into a binary image *b*(*x*,*y*)[13]:

$$b(x,y) = \begin{cases} 1, \text{ if } f(x,y) \geq k \\ 0, \text{ if } f(x,y) < k \end{cases}.$$

The optimal threshold is clearly visible in bimodal histograms, as there is a clear valley between the two peaks. This makes it easy to distinguish between foreground and background. The histograms belonging to data sets of concrete or other composite materials often cannot be easily divided into foreground and background. Therefore, the threshold k must be determined in a different way for these data sets. A common method is the Otsu thresholding. It is named after its developer Nobuyuki Otsu. This method iteratively finds the threshold at which the scatter from foreground to background is the smallest.[14]

When using Otsu thresholds in Avizo 9.5, there is the option to select an area in the histogram to search for the threshold. This makes it easier to segment different areas in data sets. Figure 7 shows the result of Otsu thresholding for the section of a data set in which the dark areas of the air inclusions have been segmented.

4 | EXAMINATION PROCEDURE

For each series of tests, 15 samples were prepared as described in Section 2.2.4. For the tests, the stress–strain curve was first determined on five samples. The measuring points for the μ-CT measurements were then determined from the stress–strain curves of these samples. Another five samples were used as backup samples in case tests had to be aborted/repeated for various reasons. The complete procedure is shown in Table 3.

4.1 | Grey value analysis

The reconstructed data sets were viewed as 3D volumes and as sectional images. In the following, the *z*-axis

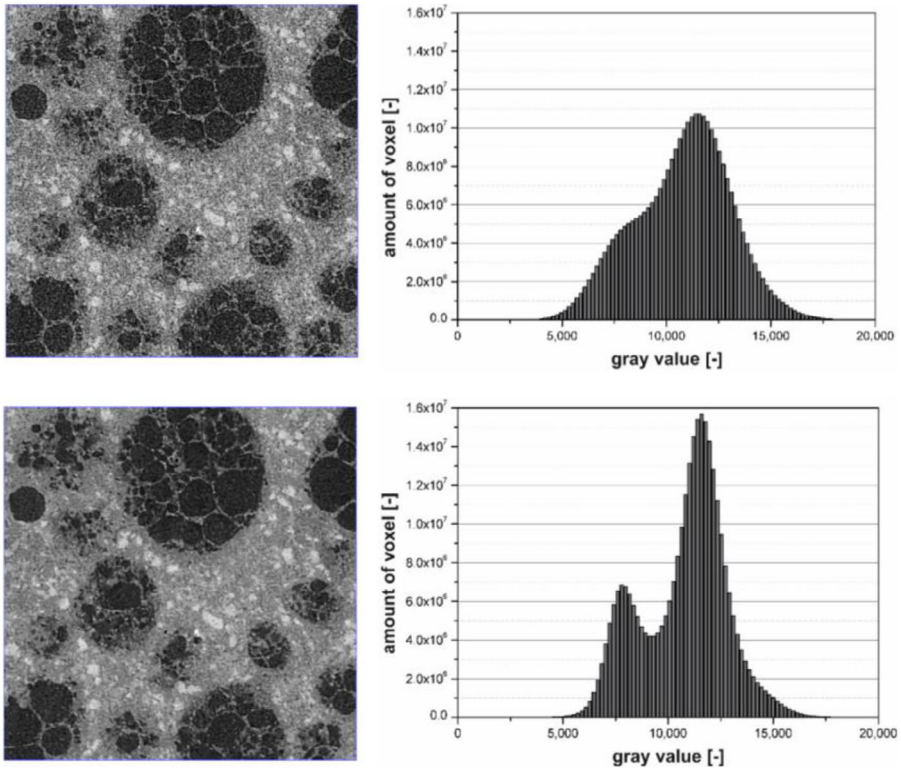

FIGURE 6 Greyscale image and histogram before filtering (top) and after the non-local means filter (bottom). The edge length of both images is 1000 μm.

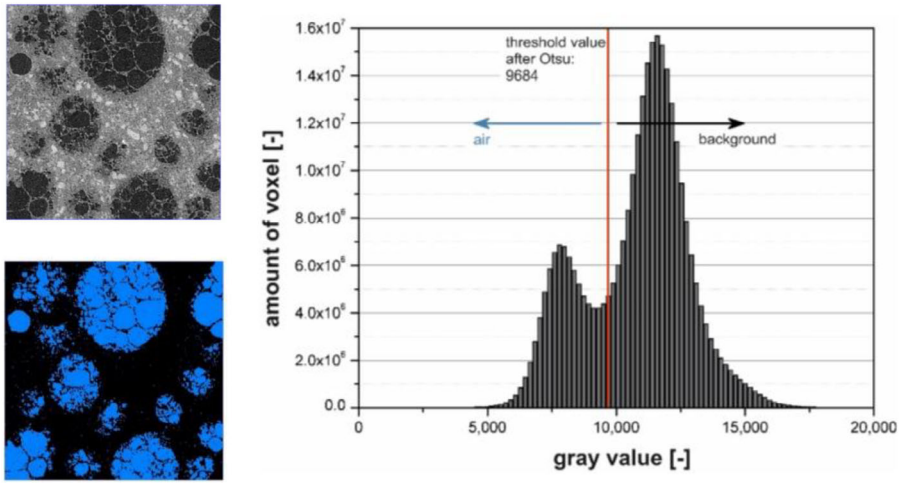

FIGURE 7 Greyscale image (left) and segmentation using Otsu thresholding (right). The edge length of both images is 1000 μm. Histogram with thresholding (bottom).

represents the direction of loading. The x and y axes span the plane. The sections are orthogonal to the axes (Figure 8). For a better overview, the sections have coloured frames:

- xy section: red frame
- xz section: blue frame
- yz section: green frame

The slices show the areas of different density. The voids are shown dark to black. In addition, the air voids are nearly spherical and uniformly coloured. The expanded glass grains, in addition, are not uniform in shape and colour. Due to the porous structure on the inside with glass nets, they appear slightly lighter in colour. Individual glass bars can also be seen in larger grains. The cement paste matrix has the highest density and appeared bright in the

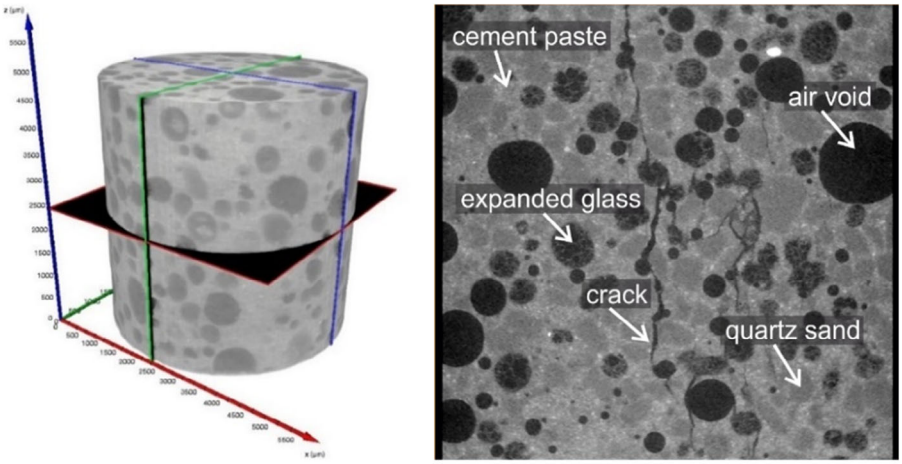

FIGURE 8 (A) Overview of the global coordinate system and the position of the sectional images, (B) overview of a CT scan with an image width of 5 mm.[15]

TABLE 3 Examination procedure.

Step	Description	Result
1	Sample preparation according to Section 2.2.4	15 samples
2	Pretests for load determination	Load values for test set-up
3	μ-CT Scans 1. Scan without load 2. Scan with approx. 30 % load 3. Scan with approx. 60 % load 4. Scan with approx. 90 % load 5. Scan after maximum stress	5 datasets in different load stages
4	Reconstruction	3D datasets
5	Filter	Filtered 3D datasets
6	Grey value analysis	Histograms
7	Change of grey values in different load steps	False colour data
8	Segmentation	Binary data
9	Analysis of binary data	Calculated parameters

μ-CT image. The quartz sand was slightly darker than the cement paste matrix. Cracks had the same colour as air and could only be recognised by their shape.

The sectional images show that the displacements and cracks are optically visible (Figure 9). In the corresponding histogram, the change in grey values can only be guessed.

In the next step, the data sets were examined for colour changes using Avizo 9.5. The software compares the colour values of individual pixels. If no colour change was detected, the pixel was displayed with a colour value of 0, that is, black. For all other pixels, the difference in colour change is added to zero.

All samples show a sickle-shaped colour shift over the pores and expanded glass (Figure 10). While the matrix is light blue in places, the quartz sand grains and much of the matrix remain dark blue. These areas are shown in similar tones of grey so that the colour shift is not apparent. The same applies to the interior of the air voids.

4.2 | Segmentation and analysis

To create a 3D model of the air trapped in the sample, several steps were performed using the Avizo 9.5 program. The different steps were always performed according to the same scheme.

First, the raw data is read into the program as a data set. The data is then cleaned using a non-local means filter. This produces the filtered data set from which the sectional images, histograms, and 3D images were taken. Up to this point, the data set consisted of grey values with stored 16-bit data. This needed to be converted into a binary image. To ensure that the decision of which voxels belong to which area does not depend on a subjective human decision, Otsu thresholding was used. This can be found in Avizo in the 'Auto Thresholding' module in the 'Factorisation' method. The upper threshold for air segmentation had to be between the first and second peak. Therefore, the calculation range was restricted and the histogram was used. The lower limit was placed before the first peak and the upper limit was placed directly in the peak tip of the second peak. The limits in which the binary image should be generated were thus found and executed using the 'Interactive Thresholding' calculation module. The thresholds only had to be calculated once for each group of measurements (measurements 1–5) because all the images were

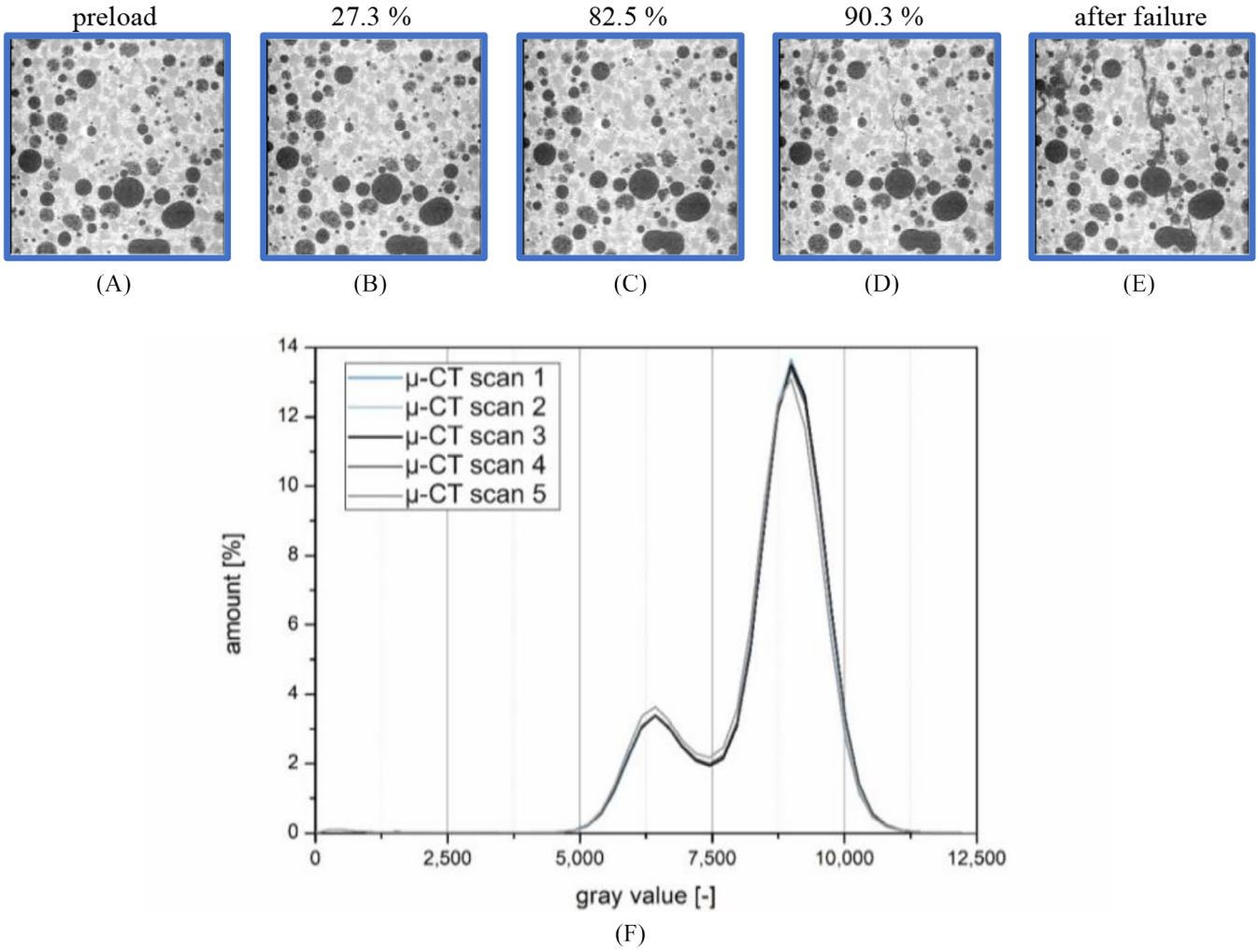

FIGURE 9 Sectional images (A–E) and histogram under different load steps[15] (F).

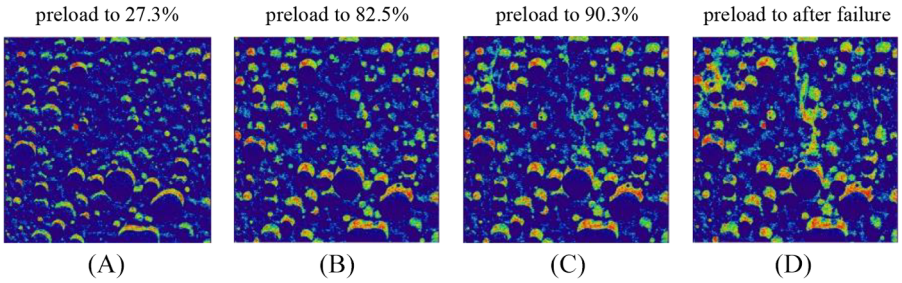

FIGURE 10 Colour shift of sample compared to the first measurement (preload).

reconstructed with the same parameters. When a binary image is created, errors appear at the edges in the form of vertical lines distributed across the surface. These are artefacts caused by the reconstruction. This is the edge area of the μ-CT image, which is why some voxels are darker there. To prevent these artefacts from affecting the model, a cylinder-shaped mask was created and subtracted from the image. Mathematically, the model now consists of 1 (object) and 0 (no object). The process of creating the model is also called segmentation, because the segments of an image are assigned to a group.

In order to calculate the geometry of individual objects, such as air pores, they must also be assigned a number. Each object that is completely surrounded by zeros

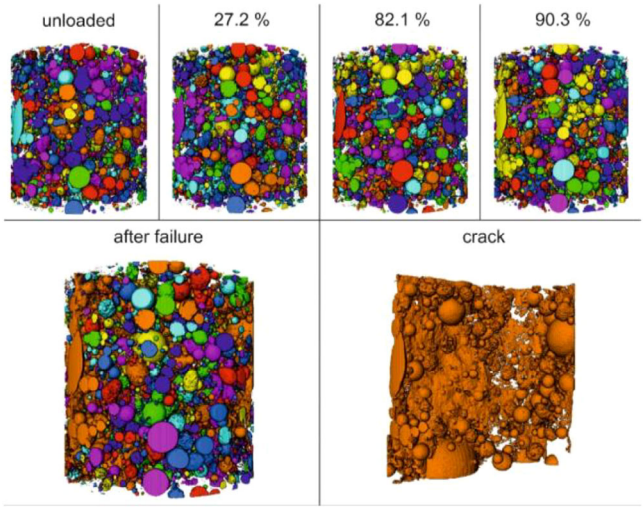

FIGURE 11 Model of the air pockets after different load conditions. Diameter of the cylinder 5 mm.[15]

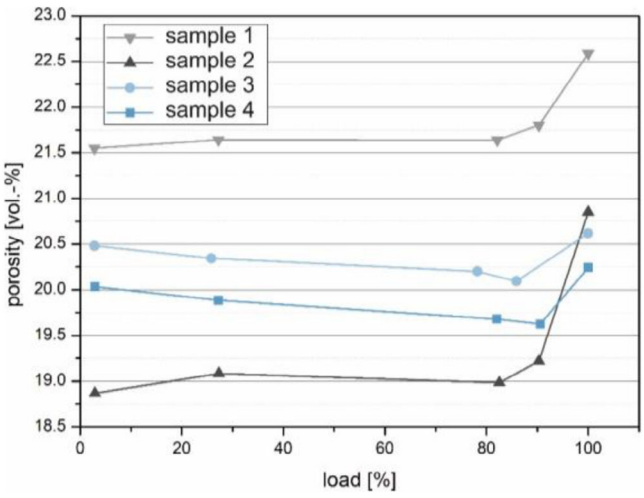

FIGURE 12 Porosity in the samples during loading.[15]

is assigned a sequential number. This process is called 'labelling'. This is illustrated visually by the different colours of the individual objects and is displayed using the 'Volume Rendering' display module. Here, eight colours are used to delineate the objects. The last step is to analyse the objects. This is done using the 'Label Analysis' calculation module.

The results of the model development can be seen in Figure 11 as a 3D image. The colour representation in the 3D models is random and determined by the program.

The porosity could be calculated from the volume at the different measurement times by comparing the sum of the segmented air inclusions to the total volume. Figure 12 shows the percentage load as a function of maximum force plotted against porosity. There are two different progressions. Samples that crack before the maximum force is reached (sample 1 and 2) tend to show a continuous increase in porosity. Samples that crack after the maximum force (samples 3 and 4) show a consolidation of the microstructure, that is, a decrease in porosity.

5 | RESULTS OF EXPERIMENTS

The fracture pattern of many samples can only be seen in the final state because no cracks or flaws were recorded in the last image before failure. Defective structures would be, for example, broken expanded glass grains or a crack. However, the samples either absorbed the load without damage or failed because the load was too close to the performance limit. The cracks that opened were unstable, resulting in a drop in stress. The load frame, which was designed to hold the set tension, attempted to restore the tension by closing the load plates, which was not possible as the cracks continued to open. This process was stopped either manually or by controlling the minimum opening width of the load frame.

The samples where stable crack growth was observed show that the cracks opened vertically in the sample, orthogonal to the load application, and had start or end points in air voids or expanded glass (Figure 13). In addition, as is often observed in UHPC, the crack propagated through quartz grains (red arrow) and at the interface (green arrow). The associated 3D model of the crack also showed the extensive branching. The red frame shows the position of the 2D section in the 3D model. After the fracture and failure of the matrix, a second crack was visible in many places next to the first crack (yellow arrow). This was wider from the crack opening than the first crack observed in this part of the sample. This indicates that tensile forces were redirected into the surrounding material and the load became too high at this location. As a result, this led to the ultimate failure of the sample.

With a resolution of 5 μm, most measurements showed little or no change in porosity in the crack volume prior to maximum load (failure). In isolated cases stable crack growth was observed. Only very small deviations in volume and shape could be measured in individual pores. One way to get more volume information would be to work with a higher resolution or improved intensity on the detector (Figure 14). The higher resolution provides a better image of the contour, while the improved intensity results in less noise and therefore fewer misclassifications of voxels. Improved intensity can be achieved by changing the voltage and power of the source and by increasing the exposure times.

With the current boundary conditions (source and detector distance, source voltage, measurement time <2 h) this is not possible. Considering the whole volume with

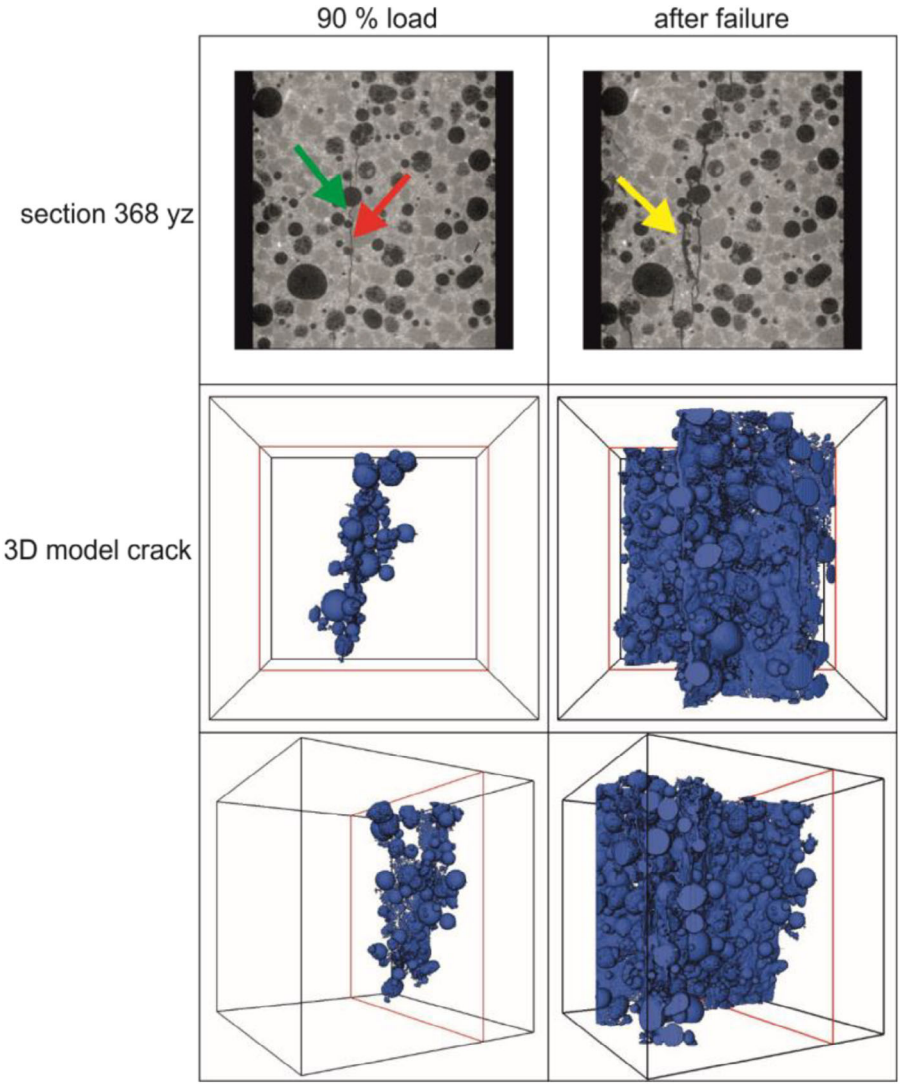

FIGURE 13 Fracture pattern of a sample at 90 % of the maximum load and in the final state. The red frame shows the position of the 2D section in the 3D model (edge length 5 mm).[15]

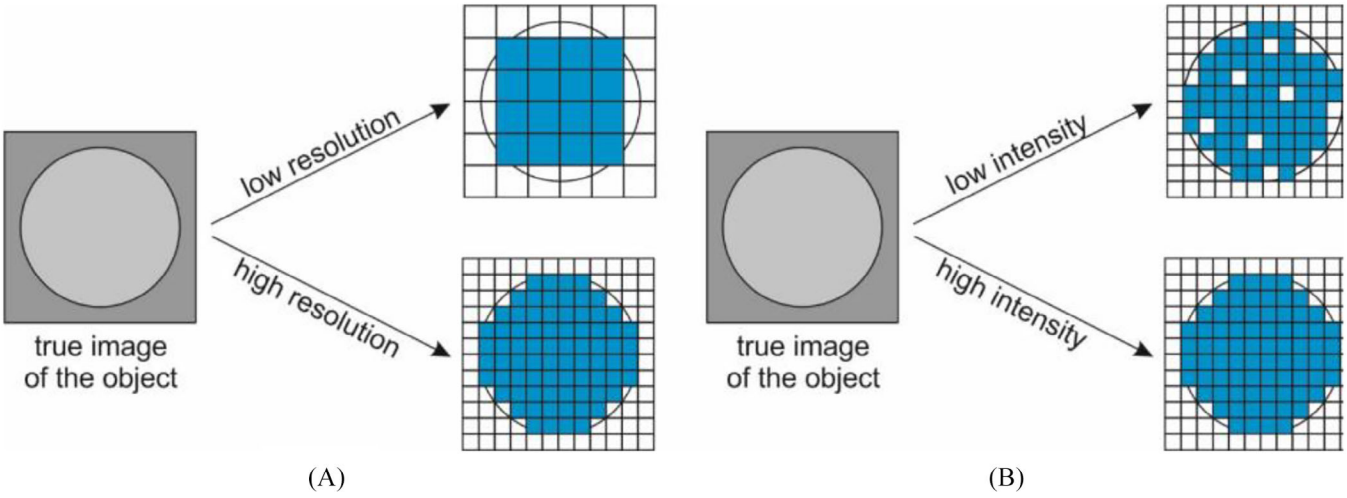

FIGURE 14 Effects of increased resolution (A) and improved intensity at the detector (B) for the segmentation of objects.

the used settings, no cracks can be observed even if the sample changes in length by 1%–1.5%. Many samples failed at the 90% measurement (4th measurement). This means that they cracked unstably under load and were crushed by the load frame. This means that only crack states that are still within the range of stable crack growth can be recorded. To measure unstable crack growth, the sample would have to be unloaded, which would also reverse the elastic deformation. This would cause some fine cracks to close again.

6 | CONCLUSIONS

In this study, the internal microstructure of lightweight concrete was investigated under load for the first time. This is only possible by using the in situ μ-CT method. Due to the large density difference between air and material, cracks could be observed even before the maximum load was applied. The in situ loading allowed the samples to be examined without intermediate unloading, allowing the microstructure to be evaluated under elastic deformation. The results of the work have provided a unique insight into the fracture behaviour of lightweight concretes, but can also be applied to other concrete systems.

In further studies, some aspects of the implementation and evaluation can be adapted. For data collection, strain was equated to machine displacement. External displacement transducers can be attached to the samples to obtain a more accurate impression of strain. However, this requires larger samples. Alternatively, strain can be determined using optical 3D surface measurement technology (GOM). The load and displacement recorded in the load frame were limited by the accuracy of the hardware. The load and displacement were within the control range of the load frame, which is 50–5000 N and 5–15 mm.

The μ-CT image acquisition is influenced by various factors (measurement parameters, sample geometry) that could not be changed in the course of these investigations and had to be kept constant. In addition to the 3D view of the samples, the advantage of μ-CT images is the option for in situ loading. Since the elastic deformation is not reversed, cracks that would close due to elastic strain can also be observed. Disadvantages of this method are the very small sample geometry and the high cost. In addition, a μ-CT can only be operated by well-trained personnel.

During the measurement, a larger measurement range could help to better detect cracks and deformations. This can be achieved either by reducing the resolution or by increasing the measurement time. Also, fewer measurement points could be selected.

The analysis of future materials should focus more on displacements than on crack initiation because, especially in high-performance materials, few cracks form before the maximum load is reached, and displacements can therefore provide a better insight into the failure process. Displacements can be determined and visualised in 3D data sets using software solutions from various manufactures. With freeware programs, like GOM Correlate (metiris GmbH, Gebenstorf, Germany), that are available today, a displacement can only be determined at selected model points. This takes a lot of time and produces less reliable results. With this method, the individual segmented objects are tracked across all measurements using the volume and position parameters. If a separation occurs due to a crack, the volume changes and the object can no longer be tracked. Another aspect is that material pores are attached to the crack models. This is due to the same density and the segmentation method. Until now, it has not been possible to remove these and display only the crack. In the future, this may be possible with AI-based analysis.

The investigations performed have significantly improved our understanding of the material behaviour of structural lightweight concrete. The expanded glass aggregate in a high strength matrix influences to the load transfer despite the large stiffness differences; the fracture is transferred from weak point to weak point by a crack. A general failure (throughout the sample – grain fracture) of the expanded glass was not observed.

In principle, the method used here is also suitable for investigating other concretes or other systems with inorganic binders and for comparing the fracture behaviour of different systems. In addition to other lightweight concretes with different bulk density classes, such as autoclaved aerated concrete, foamed concrete, and structural lightweight concrete with other lightweight aggregates, mortars with a maximum grain size of 2 mm or any high-performance concretes can also be tested.

ACKNOWLEDGEMENTS

The results presented in this paper are part of a dissertation. The dissertation was defended 30 October, 2023, at University of Kassel. The publication is available at Kassel University Press.[16]

Open access funding enabled and organized by Projekt DEAL.

ORCID

Cristin Umbach https://orcid.org/0000-0002-6795-957X

REFERENCES

1. Cusatis, G., Pelessone, D., & Mencarelli, A. (2011). Lattice discrete particle model (LDPM) for failure behavior of concrete: Part I: theory. *Cement and Concrete Composites*, *33*(9), 881–890. https://doi.org/10.1016/j.cemconcomp.2011.02.011

2. Ibrahimbegovic, A., & Delaplace, A. (2003). Microscale and mesoscale discrete models for dynamic fracture of structures built of brittle material. *Computers & Structures*, *81*(12), 1255–1265. https://doi.org/10.1016/S0045-7949(03)00040-3
3. Bazant, Z. P., Caner, F. C., Adley, M. D., & Akers, S. A. (2000). Fracturing rate effect and creep in microplane model for dynamics. *Journal of Engineering Mechanics*, *126*(9), 962–970. https://doi.org/10.1061/(ASCE)0733-9399(2000)126:9(962)
4. Oesch, T. S., Landis, E. N., & Kuchma, D. A. (2016). Conventional concrete and UHPC performance–damage relationships identified using computed tomography. *Journal of Engineering Mechanics*, *142*(12), 4016101. https://doi.org/10.1061/(ASCE)EM.1943-7889.0001168
5. Bazant, Z. P., & Planas, J. (2019). *Fracture and size effect in concrete and other quasibrittle materials*, CRC Press LLC, pp. 1–48. https://doi.org/10.1201/9780203756799
6. Buzug, T. (2008). *Computed tomography: From photon statistics to modern cone-beam CT*. Springer Verlag.
7. Du, X., & Jin, L. (2021). *Size effect in concrete materials and structures*. Singapore: Springer Verlag.
8. Talaat, A., Emad, A., Tarek, A., Masbouba, M., Essam, A., & Kohail, M. (2021). Factors affecting the results of concrete compression testing: A review. *Ain Shams Engineering Journal*, *12*(1), 205–221. https://doi.org/10.1016/j.asej.2020.07.015
9. Umbach, C., Wetzel, A., & Middendorf, B. (2021). Durability properties of ultra-high performance lightweight concrete (UHPLC) with expanded glass. *Materials (Basel, Switzerland)*, *14*(19), 5817. https://doi.org/10.3390/ma14195817
10. Deutsches Institut für Normung e. V. (2005) *DIN EN 196-1 - Prüfverfahren für Zement – Teil 1: Bestimmung der Festigkeit*. Beuth Verlag.
11. Burger, W., & Burge, M. J. (2015). *Digitale Bildverarbeitung*. Springer Verlag.
12. Buades, A., Coll, B., & Morel, J. M. (2015). A non-local algorithm for image denoising. In: *Proceedings of International Conference on Computer Vision and Pattern Recognition (CVPR)*, 2, 60–65. https://doi.org/10.1109/CVPR.2005.38
13. Süße, H., & Rodner, E. (2014). *Bildverarbeitung und Objekterkennung: Computer Vision in Industrie und Medizin*. Springer Vieweg.
14. Otsu, N. (1979). A threshold selection method from gray-level histograms. *IEEE Transactions on Systems, Man, and Cybernetics*, *9*(1), 62–66. http://doi.org/10.1109/TSMC.1979.4310076
15. Umbach, C., & Middendorf, B. (2023). Fracture behavior of ultra-high performance lightweight concrete: In situ investigations using μ-CT. *ce/papers*, *6*, 875–881. https://doi.org/10.1002/cepa.2852
16. Umbach, C. (2023). Untersuchung des Bruchverhaltens von Leichtbetonen unter einaxialer Druckbelastung mittels hochauflösender Computertomographie (μ-CT). Dissertation, Universität Kassel. Verlag: kassel univeristy press. http://doi.org/10.17170/kobra-202311169022

How to cite this article: Umbach, C., & Middendorf, B. (2024). Investigations on lightweight concrete by in situ compression tests using high-resolution computed tomography (μ-CT). *Journal of Microscopy*, *294*, 177–190. https://doi.org/10.1111/jmi.13279